

# We are IntechOpen, the world's leading publisher of Open Access books Built by scientists, for scientists

6,900

Open access books available

185,000

International authors and editors

200M

Downloads

Our authors are among the

154

Countries delivered to

TOP 1%

most cited scientists

12.2%

Contributors from top 500 universities



WEB OF SCIENCE™

Selection of our books indexed in the Book Citation Index  
in Web of Science™ Core Collection (BKCI)

Interested in publishing with us?  
Contact [book.department@intechopen.com](mailto:book.department@intechopen.com)

Numbers displayed above are based on latest data collected.  
For more information visit [www.intechopen.com](http://www.intechopen.com)



---

# The Synthesis of Nano-Crystalline Metal Oxides by Solution Method

---

Xuejun Zhang and Fuxing Gan

Additional information is available at the end of the chapter

<http://dx.doi.org/10.5772/45643>

---

## 1. Introduction

The performance of materials in many of their uses in industries and scientific researches is directly dependent on their crystal structure, which correlates to the chemical and physical properties of the materials. And also, as the size of crystal particles decrease to nanometer scale, nanocrystals exhibit some unexpected properties that are evidently different in physics and chemistry from their bulk crystals and their cluster compounds as well.

One of the most important applications of nano-materials is as catalyst to be widely used in petroleum and chemical industries, which has been a hot research area attracting high attention from researchers around the world. A lot of nanomaterials that have shown highly catalytic activity are nano-sized metal oxide crystals or doped metal oxide crystals. As well known, the nature of semiconductor is one of major features for solid catalyst, especially for solid photo-catalyst. The properties could exhibit or work as catalysts only when the metal oxide bears crystal structure. Therefore, the crystallization of oxide or doped oxide is a key step in the preparation of catalyst.

Nowadays the current processes of preparing metal oxide nanocrystal are mainly involved in sol-gel method and some modified sol-gel methods. The products synthesized by the methods, however, are metal hydroxides, which have to undergo a firing treatment (at over 350 °C) in order to have them crystallized and to be endowed with semiconductive and catalytic properties. But, the formation of oxide crystals in the roasting process involves a phase transition process, in which a new grain boundary forms and expands at high temperature, leading to size increase of the particle obtained in solution synthesis or even to a new matrix element phase from which the doping element is excluded. In addition, the process of phase transformation in calcination is unfavourable for the preparation of nuclear-shell structure of nano materials such as a magnetic nuclear coated with TiO<sub>2</sub>, SiO<sub>2</sub> or SnO<sub>2</sub>, resulting in tow-phase separation and a failure of coating on magnetic nuclear. For

the synthesis of nano-crystalline metal oxides with alterable valence, the calcination in the air causes the valence of metal to rise by oxidation and the original crystalline structure to change. And also, on the surface of the directly synthesized metal oxide nanocrystals without high-temperature burning there exists a large number of hydroxyl groups, which are more conducive to water molecules, organic solvents, or organic compounds compatible and to surface modification and functionalization of nanocrystals. See Section 4.4.

A modified sol-gel method, “precipitation–condensation with non-aqueous ion exchange (P-CNAIE)”, associating with a drying method, “azeotropic drying of iso-amyl acetate (AD-IAA)”, was put forward in 2005 (Zhang 2005), that is, in ethanol a strongly basic anion-resin was used as an exchanger to remove by-product  $\text{Cl}^-$  and as a reactant to provide  $\text{OH}^-$  for hydrolysis. The high-purity metal hydroxide tends to dehydrate in an intermolecular manner with the assistance of super water-absorbable ethanol to form crystal.

## 2. Method of synthesis

The solution chemistry method, usually referred to sol-gel method, is a significant process to synthesize the precursors of many nanoscale metal oxides. The method is widely used for it can achieve uniform doping of multi-elements no matter whether at atomic, molecular or nanometer levels at the gelatination phase. Generally, sol-gel processes have associated problems, such as difficulty in removing chlorine, and in accurate and repeated doping.

The new solution chemistry method proposed by us involves a precipitation–condensation process, with non-aqueous ion exchange in ethanol used for the removal of chlorine and for providing hydroxyl ion. (Zhang, 2005; Zhang et al., 2006, 2008; Yang et al. 2007).

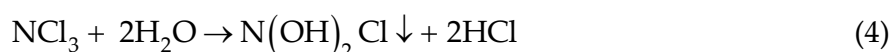
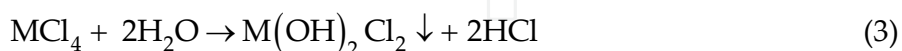
### 2.1. The underlying principle of the hydrolysis method

The method involving P-CNAIE for removal of chlorine is based on a reaction that occurs in low-polar solvents containing limited water under a slightly alkalinity condition. Generally, as the soluble metal salts dissolved in water the solution become acidic and metal ions are hydrolyzed. Such tendency is much stronger for high valence metal ions because the acidity of high valence metal ions is stronger than that of low valence metal ions. This means the  $K_{\text{sp}}$  of hydroxides of high valence metal ions are much smaller than that of low valence metal ions. Different kind of metal ion or the metal ions with different valence state have different  $K_{\text{sp}}$ ,  $M(\text{OH})_n$ , which results in a part precipitation of the metal ion with low  $K_{\text{sp}}$ ,  $M(\text{OH})_n$  in aqueous solution. That a limited amount of water is added in the organic solvent will control the hydrolysis degree of metal ions, and in this case, addition of a limited amount of ammonia water instead can both control the hydrolysis degree and avoid part precipitation of a metal ion as a doped nano- material is synthesized.

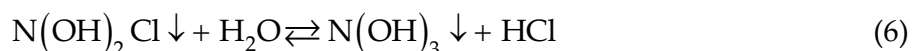
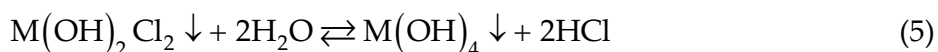
Here  $\text{MCl}_4$  is referred to as matrix metal chloride and  $\text{NCl}_3$  as metal dopant. In the synthesis, the hydrolysis takes place limitedly under the assistance of ammonia water in absolute alcohol. The acidification is attributed to the  $\text{HCl}$  coming from  $\text{MCl}_4$  and  $\text{NCl}_3$ , being caused by the first-order hydrolysis of  $\text{MCl}_4$  and  $\text{NCl}_3$ .



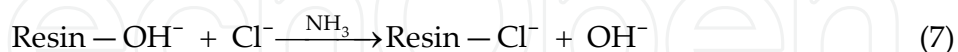
The product of the second-order hydrolysis of  $\text{MCl}_4$  and  $\text{NCl}_3$  is generally a white suspended precipitate. In an organic solvent, the polar product is precipitated much more readily, and the size of the particles is smaller because of the solubility of polar compound in organic solvent is much lower than that in water. (Wuhan U. 2000) The limited amount of ammonia water controls the rate of hydrolysis and the pH of the solution to slightly alkaline, preventing a part precipitation of either  $\text{MCl}_4$  or  $\text{NCl}_3$ :



The third- and fourth-order hydrolysis of  $\text{MCl}_4$  and  $\text{NCl}_3$  is very weak. From the third-order hydrolysis on, the pH of the solution is almost maintained at around 7 (if  $\text{pH} > 9$ , the products might be  $(\text{NH}_4)_2\text{MO}_3$  and  $(\text{NH}_4)\text{NO}_2$ , instead of  $\text{M}(\text{OH})_4$  and  $\text{N}(\text{OH})_3$ , for some amphoteric elements). The third- and fourth-order hydrolysis is reversible.

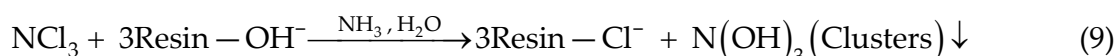
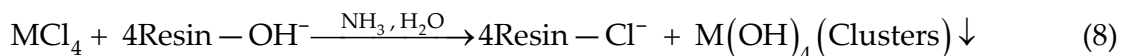


To maintain reactions (5) and (6) and prevent the formation of  $(\text{NH}_4)_2\text{MO}_3$  and  $(\text{NH}_4)\text{NO}_2$ , chlorine has to be removed under neutral or slightly alkaline conditions. This is often performed by repeatedly using a fresh neutral solvent to wash the precipitate. This process consumes considerable amount of solvent and time. However, in the process of hydrolysis using anion-exchange resin, because the affinity of the anion-exchange resin for  $\text{Cl}^-$  is over 25 times (Luliang et al., 2000) that for  $\text{OH}^-$ , the resin readily exchanges  $\text{Cl}^-$  and supplies  $\text{OH}^-$  for the hydrolysis.



This speeds up the hydrolysis and shortens the duration of time for formation of hydroxides of M(IV) and N(III).

The reaction for hydrolysis associates with anion resin can be written as



Instead of complete dispersion, the hydroxides of M(IV) and N(III) showed a tendency to dehydrate, and formed condensates. (D'Souza et al., 2000) Starting from the second-order

hydrolysis, when the monomer hydroxide has two condensable functional groups,  $f = 2$ , more and more linear condensates are formed. From the third-order hydrolysis, the average functionality of the monomer becomes more than two,  $\bar{f} > 2$ . This allows cross-linking between linear condensates, and also gelation.

## 2.2. The operation of the method

In an airtight flask containing 200 mL anion-exchange resin (say the DOWEX Monosphere 550A UPW(OH), Dow Chemical Company, Midland, MI), 100-200 mL alcohol, and 10-15 mL of ammonia water, 200-300 mL ethanol solution containing  $MCl_4$  (15-25%, w/v), or/and  $NCl_3$  (desired%, w/v) are added dropwise with fast stirring.  $NH_3$  gas was aerated in the reaction solution to catalyze the hydrolysis. The reaction apparatus is shown as Fig. 1.

The reaction solution is held close to neutral, pH 6-8, by adjusting the speed of addition. After the addition is complete, a solution containing a white suspended precipitate is separated with resin through a glass-sand funnel or a 120 mesh stainless steel screen. The filtrate reacts repeatedly with 50-100 mL fresh anion-exchange resin on a shaker, to continue removal of chlorine and promote further hydrolysis for five or six times until the upper solution does not become clear upon standing and  $Cl^-$  in solution is not detected by More Essay. The final chlorine-free (checked by  $AgNO_3$  solution) colloid solution is held idle on a bench for ca. 48-72 h and separated into an upper lightly turbid solution and a lower dense precipitate. The upper, lightly turbid solution is then removed and kept aside for final recovery of all precipitate. Iso-amyl acetate (70-100 mL) is added to the lower dense precipitate solution to make a co-boiling system. A dispersive fine powder is obtained by co-distilling off water absorbed on the colloid and solvents, or azeotropic drying.

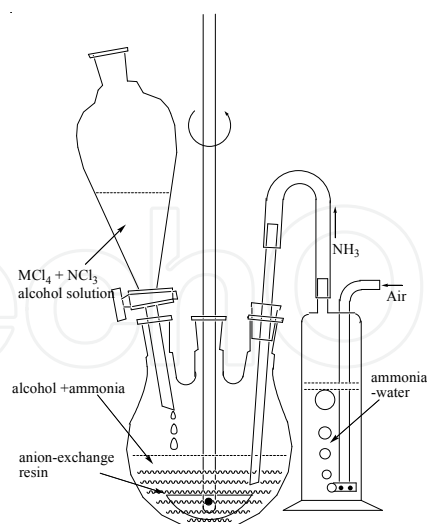


**Figure 1.** The glass apparatus for preparation of doped nanocrystal by hydrolysis of  $MCl_4$  and/or  $NCl_3$ .

All the exchanged ion-exchange resins are combined and repeatedly washed with fresh solvent to collect any residual precipitate on the surface of the resin. The washed solvent is applied to a short column of ion exchange to remove any remaining chlorine, and is then combined with the upper lightly turbid solution. The resulting dried powder is then

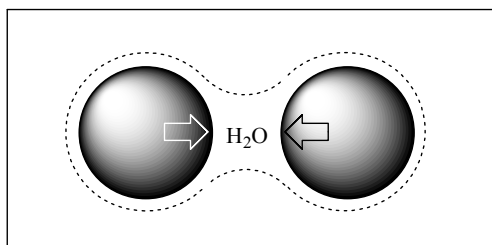
dispersed in the combined solution on a shaker, and a chlorine-free solution containing powder is distilled to separate the solvent and leave behind the hydrolysis product, as a high-dispersively fine powder.

### 2.3. The drying of nano-crystalline metal oxides

To coupling with the method “P-CNAIE”, a drying method of “azeotropic drying of iso-amyl acetate (AD-IAA)” was presented in 2005 (Zhang, 2005; Yang et al., 2007)

Although the solution chemistry method is a significant process to synthesize many nanoscale metal oxides, the drying methods plays a key role in the successful preparation of nanoparticles. If the surface tension is not reduced (Sun & Berg, 2002) during the drying process of precipitate colloids, the colloid particles will aggregate to form rigid gel pieces in the end. It has been known that gels can be formed either through the condensation of polymers or through the aggregation of particles (Diao et al., 2002). According to cluster-cluster growth models, clusters stick together randomly with a certain probability upon colliding (Brinker & Scherer, 1990). It is found that cluster-cluster growth resulting from colliding may occur easily at the drying stage. Although dried gel bulks can be ground to powder, the mechanical force cannot crush them into the powder as fine as the particles synthesized. In addition, the ground powder displays structural features different from the original colloid-precipitated particles. Thus, along with the synthesis process, the drying process is critical in determining the dispersivity and size of the final dried products in the solution chemistry process (Richards & Khaleel, 2001).

Several drying methods, such as supercritical drying (Boujday et al., 2004; Park et al., 2002), freeze drying (Vidal et al., 2005; Shlyakhtin et al., 2000), microwave drying (Hwang et al., 1997), and azeotropic distillation (Hu et al., 1998; Frazee & Harris, 2001; Luan et al., 1998) have been developed to remove the trace of water adsorbed on the surface of colloid particles in order to prevent or reduce aggregation caused by shrinkage of water films between precipitated particles. The water film is formed by adsorbing water on the surface as colloid particles contact. See Scheme 1. Supercritical, freeze, and microwave drying methods reduce agglomerates by eliminating or reducing the surface tension of the water films between colloids. Azeotropic distillation, however, removes the adsorbed water on the surface as colloids disperse in an azeotropic solution, thereby preventing the formation of water films between colloids and aggregation of particles. Some surfactants can prevent colloids from aggregating, but they have a high boiling point and are adsorbed on the dried powder so tightly that it is hard to be removed by the normal drying process.



**Scheme 1.** Particles come close up as water films between particles shrink at final drying stage.



### 2.3.1. The effects of boiling point and molecular structures of azeotropic agent on the dispersivity and fluffiness of the dried powder

We have ever presented our results from a series of azeotropic solvents such as alcohols, ethers, and esters. It is found that the molecular structures of azeotropic agents have a strong influence on the dispersivity and fluffiness of the dried products.

Experiments have demonstrated the existence of water on the surface of colloid particles by the separated water phase below the organic solvent layer in the bottle collecting condensed fluid at the azeotropic distillation stage. The water is introduced into the hydrolyzed solution by the added ammonia water, and from the condensation reaction of hydrolysate and the crystal water of metal chlorides. The surface-hydrated layer of particle confers the polymer precipitate colloid with a stable dispersivity in the ethanol. During evaporation, the ethanol is evaporated first and water molecules are left on the surface of the precipitate particles. As colloid particles come together, surface-hydrated waters combine with each other to form a water film between the particles. The film water, like capillary one, has capillary forces that can cause water film to shrink and particles eventually to contact each other and form hard brown agglomerates, for Sb-doped  $\text{SnO}_2$  nano particles see Fig. 2(A).

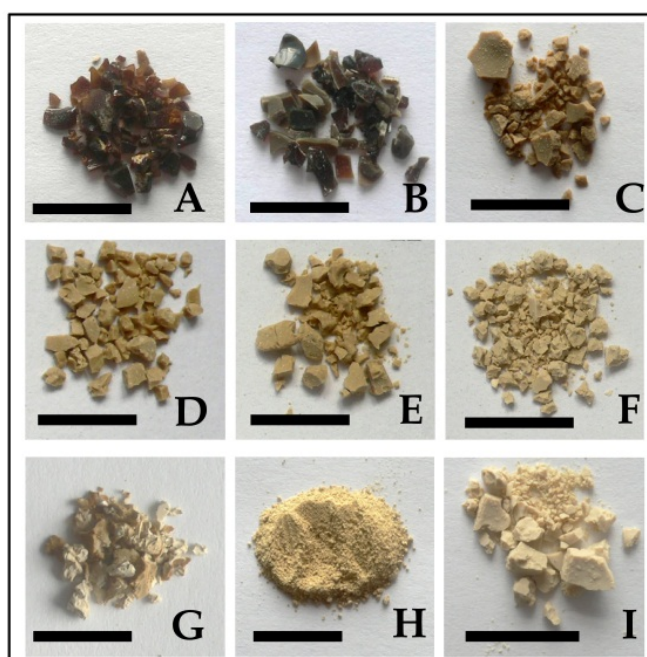


**Figure 2.** Images of antimony-doped stannic nanocrystal that is dried directly by distilling ethanol off (A) or dried by azeotropic distillation with 1,4-butanediol (B); ethylene glycol–monomethyl ether (EGMMeE) (C); n-butanol (D); pentanol (E); iso-amyl alcohol (F); tetrachloroethylene (TCE) (G); n-butyl ether (H); and n-butyl acetate (I). The scale of bar in pictures is 1.0 cm. (Zhang, 2005; Yang et al., 2007)

To remove the water molecules on the particles and keep the colloid particle dispersed, some organic solvents in Table 1 are selected. The characterization of the dried samples in Fig. 2 is summarized in Table 1. The number of symbol + stands for different grade color, agglomerates, and hardness. It can be seen that when short-chain organic solvents with two oxygen groups are used as azeotropic agents, the properties of the dried products (Fig. 2(B)

and (C)) are similar to that without azeotropic treatment (Fig. 2(A)), meaning that they play the same roles as water molecule, leading to semi-transparent xerogel pieces (Figs. 2(A) and (B)). Here, the rigid gel is formed through the aggregation (Brinker & Scherer, 1990).

Even though the dense precipitate solution is shaken with TCE or n-BuE vigorously, once shaking is stopped, the mixture immediately separates into a colloid precipitate phase and a clear solvent phase, implying that the solvents with functional groups  $-\text{Cl}$  and  $-\text{O}-$  cannot form stable H-bond with surface water molecules or surface  $-\text{OH}$  (see Table 1). When the mixtures are dried under an infrared lamp, grinding can disperse wet agglomerates into small particles and dried fine dust is obtained (see Fig. 2(H)), but the wet agglomerates become hard dried agglomerates without grinding (see Fig. 2(G)). The sedimentation experiments of colloid particles in other solvents have demonstrated that colloid particles can disperse well in these organic solvents with  $-\text{OH}$  or/and  $-\text{COO}-$ , suggesting that there are stable H-bonds between the functional groups and water molecules or  $-\text{OH}$  on the surface of the colloid.

Compounds	<i>D.</i> (g/mL)	BP °C	Groups	Molecular Wt. (no groups)	Characteristics of dried product		
					Color	Agglomerates	Hardness
Ethanol		78	$-\text{OH}$	29.06	+++++	+++++	+++++
1,4-Butanediol	1.016	235	2- $\text{OH}$	56.10	+++++	+++++	+++++
EGMMeE	0.964	124	$-\text{OH}, -\text{O}-$	43.09	++++	+++++	++++
TCE	1.622	122	4 $-\text{Cl}$	24.02	+++	++++	++++
n-Butanol	0.810	117	$-\text{OH}$	57.11	+++	+++	+++
n-Pentanol	0.815	138	$-\text{OH}$	71.14	+++	+++	++
i-Amyl alcohol		132	$-\text{OH}$	71.14	++	++	+
n-Butyl acetate	0.881	126	$-\text{COO}-$	84.16	+	++	+
n-Butyl ether	0.769	142	$-\text{O}-$	114.23	++	+	++

a: Five plus indicates that colour is the deepest, agglomerates are the most, and hardness is the highest.

**Table 1.** Characters of products azeotropically dried by different solvents <sup>a</sup>.(Zhang, 2005)

The characteristics of the dried products prepared using n-pentanol, i-AmAl (i-Amyl alcohol), or n-BuA as an azeotropic agent have some differences, which, it is assumed, result from the differences in their molecular structures. Although compared with n-pentanol, i-AmAl is a more effective azeotropic agent and the obtained dried product is fluffier. However, the dried product treated by n-BuA is fluffier than that treated by i-AmAl. These results indicate that the improvement of fluffiness results from the molecular steric structure. n-BuA has the highest steric effect. Its two side chains stretch out and cover more surface area of colloid particles to prevent the particles from contacting each other. All of these suggested that the capacity of the azeotropic agent to remove water adsorbed on the surface of the colloid depends not only on its boiling point but also on its ability to replace the surface water molecules and indicated that the dispersivity and fluffiness of the dried product are controlled by the steric effect of the azeotropic agent. In this case, an effective azeotropic drying agent may be called an azeotropic dispersing agent.



The trends of dispersivity and fluffiness of the dried products changing with the functional groups and molecular structures of azeotropic solvents are shown in Fig. 3. Some empirical rules for selecting an azeotropic agent are drawn as follows: (1) the solvent molecule should contain at least one oxygen as the H-bond acceptor to form H bonds with the surface –OH of the polymer particle; (2) the H-bond acceptor should locate in the middle of the alkane chain rather than on the terminal so that the alkane can stretch out and cover more surface area; and (3) solvents should have a higher boiling point ( $\sim 140^\circ\text{C}$ ) to reduce the time of azeotropic distillation and the residual amount of azeotropic agent.

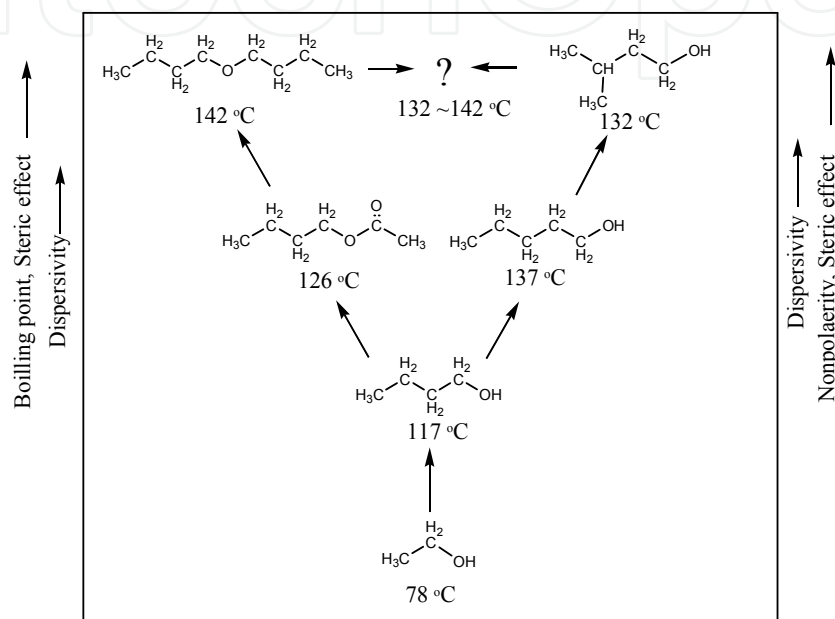


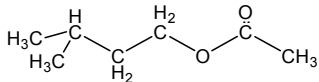
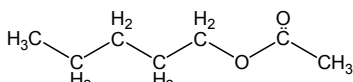
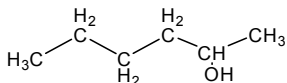
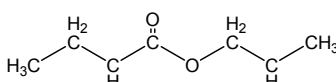
**Figure 3.** The variation of dispersivity and fluffiness of dried products with the groups and molecular structures of azeotropic solvents. (Zhang, 2005)

### 2.3.2. Iso-amyl acetate as an azeotropic agent (Zhang, 2005; Yang et al., 2007)

The empirical rules and Fig. 3 guide us to find some other new organic azeotropic solvents for both drying and dispersing. Except for 2-hexanol, the other three organic solvents in Table 2 should have similar capacities of drying and dispersing colloid particles. The i-AmA (iso-Amyl acetate) is chosen as azeotropic solvent for it is commercially available and cost-effective among the three solvents. The behaviors of mixtures combining i-AmA with dense precipitate solution are monitored and measured carefully. (Yang et al., 2007).

The analysis of specific surface area of dried product is conducted for further substantiating the effects of i-AmA on the dispersivity. The adsorption isotherms are displayed in Fig. 4. The BET nitrogen surface areas are obtained by applying the BET equation to a relative pressure range of 0.05–0.3 on the adsorption isotherm. It can be seen that the BET surface area increases from 234.75 to 286.43  $\text{m}^2/\text{g}$  as the azeotropic solvent changes from the often-used n-butanol to i-AmA, and the dispersivity of the dried powder increases by 22%. Before the adsorption measurement, the dried product, large pieces of dried agglomerates,

obtained with n-butanol has to be ground. However, the dried product from i-AmA is a highly dispersed powder such that it does not need further grinding, see the TEM images in Fig. 8. The IR spectrum of the dried powder derived from i-AmA shows lower residual organic compounds. XRD patterns and TEM images suggest a high mono-dispersivity of dried powder. These findings indicate that i-AmA is a much better azeotropic agent than other organic solvents.

Solvent	Structure	Group	MMWt.	b.p.(°C)	D.(g/ml)
iso-Amyl acetate		-COO-	98.19	143	0.88
n-Amyl acetate		-COO-	98.19	149	0.88
2-Hexanol		-OH	85.17	140	0.83
Propyl butyrate		-COO-	98.19	142	0.88

**Table 2.** Structures and physical properties of the selected organic solvents. (Zhang, 2005)

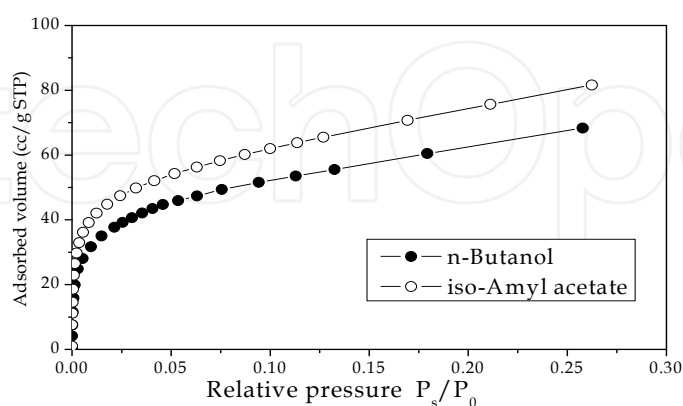
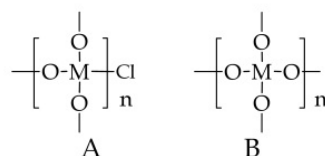


**Figure 4.** Nitrogen adsorption isotherms for dried Sb-doped SnO<sub>2</sub> powder on the SA3100 made by Becjman-Coulter co. USA. (Yang et al., 2007)

### 3. The formation of crystal particle in the process of synthesis (Zhang, 2008)

#### 3.1. Functions of anion-exchange resin

The anion-exchange resin accelerates the hydrolysis of metal chloride, which is quite significant for the hydrolysis of the third- and fourth-order hydrolysis of  $MCl_4$  and  $NCl_3$  because the hydrolysis is reversible. However, if the removal of chlorine from hydrolyzate is carried out by washing with water or organic solvent, the hydrolysis will be a slow and a long-term process. When the number of group  $-OH$  borne by an atom  $M$  or  $N$  is more than two, condensation will take place between molecules by inter-molecularly dehydrating, or even gelatination occurs. The gelatination has the polycondensate form, a space network structure. The structure hinders the complete removal of fourth- or even third-order chlorine from gel and, therefore, can not lead to the formation of crystal of metal oxide because the remained chlorines block the condensation. See Scheme 2 A.



**Scheme 2.** The condensation of hydrolysis product.

The anion-exchange resin has a much higher affinity for  $Cl^-$  than for  $OH^-$ , if once bonding a chloride ion to itself and a hydroxyl ion is given off to keep a constant concentration of  $OH^-$ . Due to anion-exchange resin can remove  $Cl^-$  completely from solution, in this case, the hydrolysis product is high purity, which is of great advantage for the condensation of metal hydroxide to form crystal or assume a crystalline structure. See Scheme 2 B.

Another important function of ion-exchange resin is to crush masses of gel to nanoparticles like small balls in the Ball Grinder as the removal of chlorine is carried out on a shaker. In this way, the removal of chlorine from nanometer-sized particles is easy, fast, and efficient, which provides the condensation and crystallization with metal hydroxides bearing high purity. And also the function of the ion-exchange resin pellet analogous to that of ball milling results in a synthesized product with a nano-meter size and a very narrow size distribution.

Moreover, the removal of chlorine by ion-exchange resin instead of by repeated changing fresh solvent is of great importance to be used for accurate and repeated doping and for preparing nanocrystals with a narrow size distribution.

#### 3.2. Functions of ethanol as solution medium

In the synthesis, the absolute ethanol is selected as a solution medium. Generally, metal salts, especially high valence metal salts, hydrolyzes evidently when they are dissolved in water, contributing to an acid reaction solution that causes precipitation (segregation) of

some metal salts as the doping is conducted. In addition, since a lot of metal salts have fast hydrolytic reaction rate, the use of water as solvent leads to an uncontrollable hydrolysis speed and a great deal of hydrolyzate settlement and agglomeration in a short time, which increases the difficulty of complete removal of chlorine from solid precipitates. A limited amount of water can control the hydrolytic rate under the ammonia as a controller of pH and the strongly anion exchange resin as a donor of  $\text{OH}^-$ .

The crystallization process in the solution synthesis of nanocrystal of metal oxide is essentially an inter-molecular dehydration process of metal hydroxides. A large quantity of water existing in the reaction system will definitely slow or even stop inter-molecularly dehydrating of the hydroxides. Ethanol, as been well known, is born with a strongly hygroscopic property and will pull water away from metal hydroxide to have it form oxide crystal. The water as a carrier of  $\text{OH}^-$  between metal salt and ion-exchange resin, see reaction formula (8) and (9), is limited, whereas a large excess of ethanol plays an important role in promoting the crystallization by seizing water molecules from metal hydroxides, especially the promotion effect of ethanol is highly effective as the hydrolysis product is milled to nanometer size by ion-exchange resin balls on a shaker.

### 3.3. Behaviours of hydrolysis products and the crystal forming process in synthesis

The hydrolysis of many metal salts using the method of "P-CNAIE" follows some regularity. The stability of hydrolysis product colloid and the solution viscosity are related to the remains of chlorine in the hydrolysis solution, as shown in Fig. 5 and 6, which show the behaviours of the hydrolysate produced from  $\text{SnCl}_4$  doped with  $\text{SbCl}_3$  and from  $\text{ZnCl}_2$  doped with  $\text{SbCl}_3$ . The left ones in both figures are the settlement ratio of hydrolysate in 2 h and right ones are the variation of the relative viscosity of solution containing hydrolysate.

We believed that the process of synthesizing nanocrystal undergoes three stages as shown in Fig. 7. At the first stage the sol, or linear molecule, is formed since where the sol is just the product of the first- and second-order hydrolysis of  $\text{MCl}_4$  and  $\text{NCl}_3$ , which corresponds to the A to B in left figures of Fig. 5 and 6. The sol particles grow as the third- and fourth-order hydrolysis of  $\text{MCl}_4$  and  $\text{NCl}_3$  occurs and settle down at the bottom of the container at the second stage, corresponding to the line CD in the left figures in Fig. 5 and 6. Whereafter, the obtained precipitate is kept on reacting with ion-exchange resin to remove the remained chlorine and the precipitate re-suspends in ethanol solution at the third stage, as line EF in the left figures in Fig. 5 and 6. Here a further condensation takes place, leading to the contraction inward of particles and formation of nanocrystal in their central core.

Fig. 7 indicates that when the surface of precipitates bears a same material or electric charge (chlorine or water) precipitates become colloids suspending in solution. The phenomena are more evident for high valence metal than low valence metal. But for the alkali rare metal (such as Lanthanum) the hydrolyzate is unstable and readily settles down.

The variation of viscosity is evidence that substantiates the growth of sol in the synthesis of nanocrystal. The increase of the relative viscosity,  $\eta_r$ , of reaction solution shows the increase

of the internal friction of hydrolysate, thus indicative of the increase of polymerization degree, or molecular weight, of hydrolysate. The successive ion exchanging does not add the molecular weight but cause the hydrolysate condensate inwards and internal friction decrease, contributing to relative viscosity drop. The inward condensation of particles accompanied by the dehydration between linear polymers is the crystallization process of colloid particles.

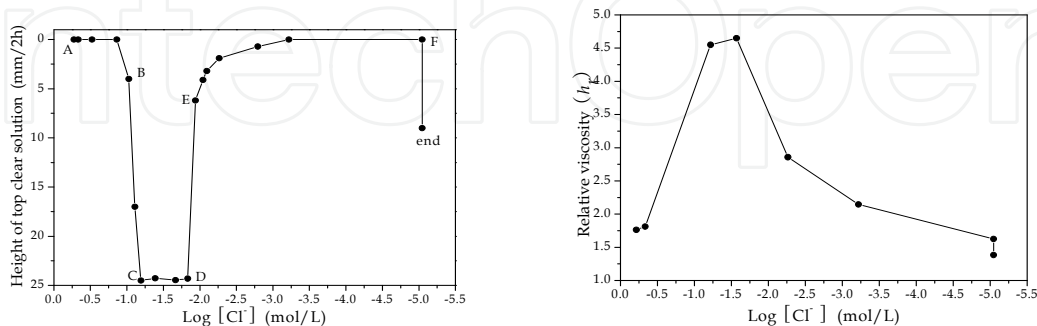


**Figure 5.** The stability of colloid in solution, see the left, and the solution relative viscosity,  $\eta_r$ , see the right, vary with  $[\text{Cl}^-]$  in hydrolysis of  $\text{SnCl}_4$  doped with  $\text{SbCl}_3$ . (The low limit of More Essay is  $9 \times 10^{-6}$  mol/L for  $\text{Cl}^-$ ).

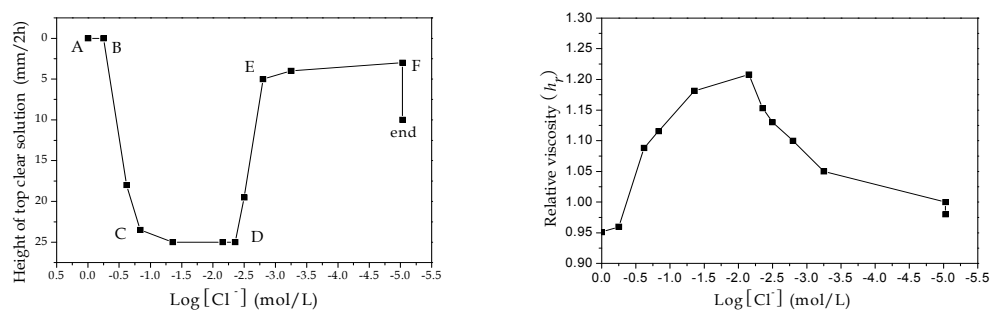


**Figure 6.** The stability of colloid in solution, see the left, and the solution relative viscosity,  $\eta_r$ , see the right, vary with  $[\text{Cl}^-]$  in hydrolysis of  $\text{ZnCl}_2$  doped with  $\text{SbCl}_3$ . (The low limit of More Essay is  $9 \times 10^{-6}$  mol/L for  $\text{Cl}^-$ ).

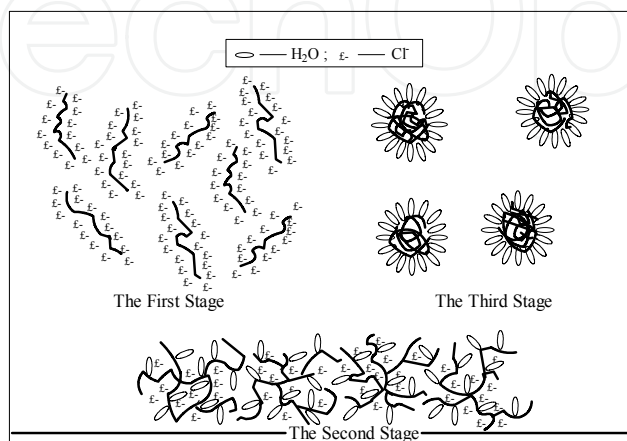


**Figure 7.** The three stages in the hydrolysis process of  $\text{MCl}_4$  (or mixed with  $\text{NCl}_3$ ).

## 4. Nanocrystal of stannic oxide doped with antimony

Nanocrystalline Sb-doped  $\text{SnO}_2$  has many merits of stable chemical, mechanical, and optical properties and environmental stabilities. The introduction of the Sb element in the tin oxide lattice confers good conductivity to the materials and an extremely high potential of evolving oxygen in water. Moreover, the nanocrystalline Sb-doped  $\text{SnO}_2$  has the potential to catalyze decomposition and oxidation for esters and alcohols. (Richards et al., 2001)

Binding energies of electrons and bandgaps between valence bands and conduction bands of materials are two significant parameters determining the properties of materials. Both are highly associated with the doping and the physical dimension of the material. The method of "P-CNAIE" can be used for accurate doping and to synthesize nanocrystals with a narrow size distribution because uniform and accurate doping at atomic or molecular levels confers stable and reliable properties and size of nanocrystals is associated with different quantum confinement effects (Yoffe 1993).

### 4.1. The synthesis

In an airtight flask containing 200 mL anion-exchange resin, 100 mL alcohol, and 10 mL of ammonia water, 200 mL ethanol solution containing  $\text{SnCl}_4 \cdot 5\text{H}_2\text{O}$  (18.0%, w/v) and  $\text{SbCl}_3$  (0.665%, w/v) are added dropwise with fast stirring. At the same time,  $\text{NH}_3$  gas is aerated in the reaction solution (see Fig. 1 and Zhang et al. 2006). The reaction solution is held close to neutral by adjusting the speed of addition. After the addition is complete, a reaction solution is separated with resin through a glass-sand funnel and reacts repeatedly with 80 mL fresh anion-exchange resin on a shaker. The white precipitate gradually become light yellow during shaking. The final chlorine-free colloid solution is held idle on a bench for ca. ~48 h and separates into an upper lightly turbid solution and a lower dense precipitate. The upper lightly turbid solution is removed and kept aside for final recovery of all precipitate and the lower dense precipitate slurry is added ~80 mL of iso-amyl acetate to make a co-boiling system. A light-yellow dispersive fine powder is obtained by co-distilling off water absorbed on the colloid and solvents.

All the exchanged ion-exchange resins are combined and repeatedly washed with fresh solvent to collect any residual precipitate on the surface of the resin. The washed solvent is applied to a short column of ion exchange to remove any remaining chlorine, and is combined with the upper lightly turbid solution, in which, then, the resulting dried powder is dispersed on a shaker. In succession, the chlorine-free combined solution is distilled and leave behind a fine light-yellow powder. In this way, all of the metal hydrolysate can be recovered and an exact doping as experimenter desires is achieved.

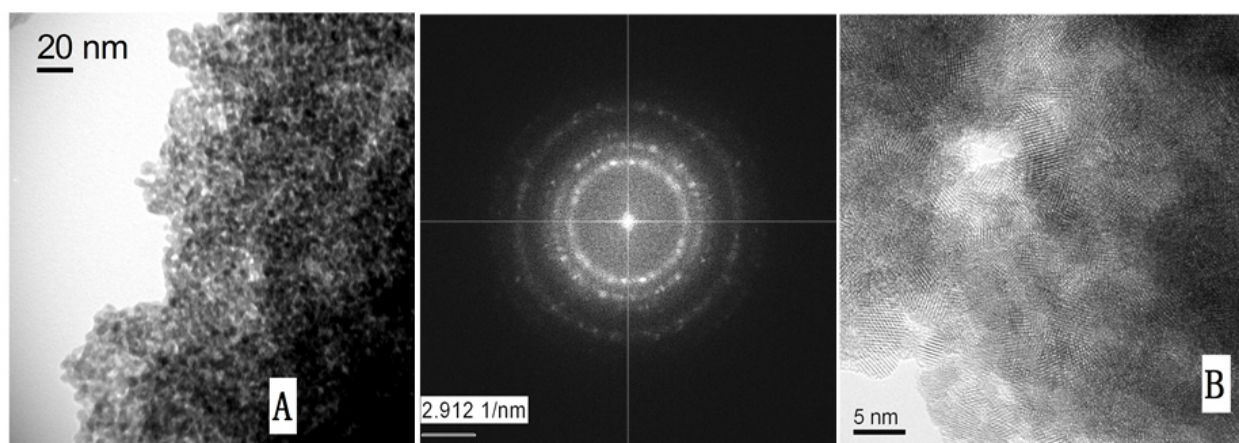
### 4.2. The characterization of the structure

Fig. 8 shows TEM images and electron diffraction pattern of nano-meter sized material synthesized by the method "(P-CNAIE)" associating with "(AD-IAA)". The electro diffraction pattern in Fig. 8 indicates that the obtained nanomaterial has a determinate



crystal structure, which is also confirmed by the TEM image B, from which a layer lattice structure can be distinctly identified.

In addition, XRD pattern in Fig. 8 illustrates the degree of crystallization and the size of nano particle. Diffraction peaks and their position in the pattern indicate the nano material is stannic oxide crystal, and broad and weak peaks suggest the size of the crystal is nano-meter sized. The positions of peaks are consistent with that showed in the X-Ray Powder Diffraction Standards of  $\text{SnO}_2$ , PDF No. 41-1445 from Jade 5.0, see the red bar in Fig. 9. Fig. 10 is the TEM image of the finally fine powder treated at  $650^\circ\text{C}$  for 3 h. It is quite obvious that the treatment at high temperature increases the size of nanoparticle in comparison with the size showed in Fig. 8A. Nevertheless, the dispresivity of both nanomaterials, unburned and burned, is almost the same.



**Figure 8.** The TEM photoes of Sb-doped  $\text{SnO}_2$  nanomaterial synthesized by method of P-CNAIE associate with AD-IAA and the EDP picture (JEM-2010FEF, JEOL, Japan). (Zhang, 2005)

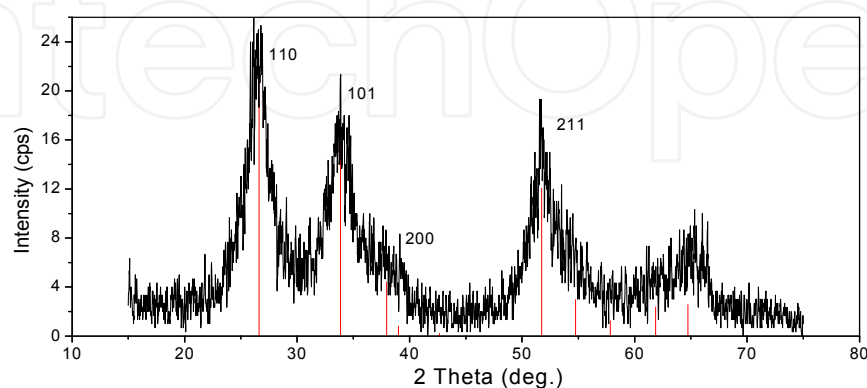


**Figure 9.** X-ray diffraction of Sb- $\text{SnO}_2$  nanomaterial synthesized by method of P-CNAIE associating with AD-IAA.

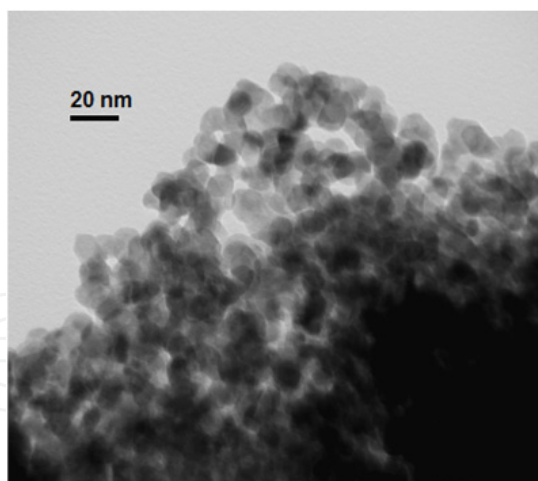


**Figure 10.** The fired Sb-SnO<sub>2</sub> nanomaterial synthesized by method of P-CNAIE associate with AD-IAA at 650°C. (Zhang et al., 2006)

### 4.3. The conductivity

#### 4.3.1. Accuracy of doping

To achieve a stable and reproducible conductivity of Sb-doped SnO<sub>2</sub>, an accuracy of doping is critical. By the method of “P-CNAIE”, it was observed that initial white precipitate gradually became final yellow dried powder. Whereas, without doping, hydrolysate of pure stannic chloride from initial colloidal to final dried powder is always white. These implicate: the yellow color is caused by Sb doping into condensate of stannic oxide, or, exactly, by Sb doping into crystal lattice of stannic oxide, because yellow is caused only by crystal with variation of band gap but by cluster or hydrolysate with forbidden band.

Because of the intermolecular condensation of hydroxides, the fine powder has no fixed chemical formula and, therefore, the total weight of the powder had to be multiplied by a conversion factor,  $r'$ , which is a ratio of the conversion, associating with the crystallization, of hydroxide into oxide, see Section 6, in order to calculate the content of Sb in an oxide crystal. A fired antimony-doped stannic hydrolysate at >350 °C does not dissolve in acid or basic solution and the method of fusing it with caustic soda results in serious errors, so the fresh dried powder is dissolved in HCl solution to make a sample for AAS. Fig. 11 shows a histogram of the content comparison of antimonies in powders and in reaction solutions before hydrolysis. The figure shows a high similarity between samples before and after the hydrolysis, within the molar fraction range of 0.040–0.075, and the highest relative error is only 1.24% (see Fig. 12).

It is not clear what causes the larger errors in the low-molar fraction range for Sb. It may be that the smaller low condensate of stannic hydroxide is more readily absorbed on the resin and difficult to be washed off with solvent. Or possibly, when being placed in the AAS, the sample was not atomized well, leading to an increase in the absorbing area of Sb and a high light absorption.

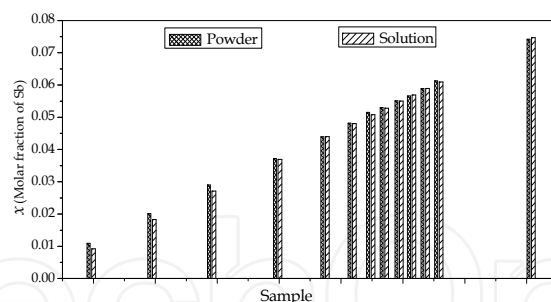


**Figure 11.** The comparison of Sb content in powders and in solutions before preparation reaction. The contents of Sb were detected on an atomic absorption spectrometer.

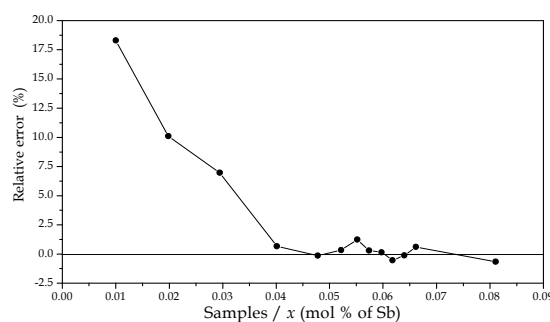


**Figure 12.** Relative errors in powder sample based on the content of solution before reacting.

Using anion-exchange resin to remove chlorine not only increased the recoverable yield but also ensured the accuracy and the similarity of doping, since the removal of chlorine is always carried out in the same solution. The only thing that needs to be replaced is the resin. Although there might be a small amount of precipitate absorbed on the surface of the resin, it can be washed off by shaking repeatedly with a fresh solvent and recovered by distilling off solvent. The worst aspect of removing chlorine by solvent washing is that the ratio of Sb to Sn is not fixed, whereas, in ion-exchange method, the proportion of Sb present in the solution before the reaction and in the powder are identical.

#### 4.3.2. Effect of doping on the conductivity

$\text{SnO}_2$  is a semiconductor with a wide bandgap ( $E_g = 3.97$  eV) and transforms into a conductor after being doped with antimony (Grzeta et al., 2002). Our process provides a method to vary the content of Sb accurately. The ordinate in Fig. 13 indicates the logarithmic value of the resistivity of samples. There is an optimum ratio of Sb to Sn that gives the lowest resistivity, ranging between 5.28 and 5.50 mol% Sb, or 5.41 and 5.63 wt% Sb.

The variation of the resistivity of Sb-doped  $\text{SnO}_2$  can be explained by the semiconductor fundamental theory. As the content of Sb increases and the density of the carrier and the carrier mobility,  $\mu$ , increase, the room-temperature resistivity of the crystal decreases. However, when the level of Sb is in excess of 5.50 mol%, as the carriers move in the

semiconductor, the ionized impurity scattering can no longer be neglected. The increase in the number of scattering centers with addition of more antimony increases the amount of ionized impurity scattering and correspondingly decreases the carrier mobilities, which in turn increases the resistivity. Especially, the heavy doping will result in Burstein–Moss effects, which cause the bandgap to become wider (Cao et al., 1998; Irvin, 1962).

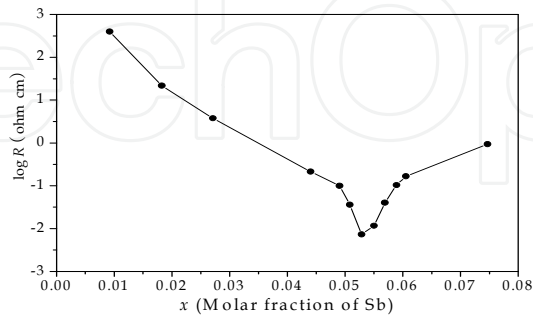


**Figure 13.** The variation of resistivity of Sb-doped  $\text{SnO}_2$  with the content of Sb in it.

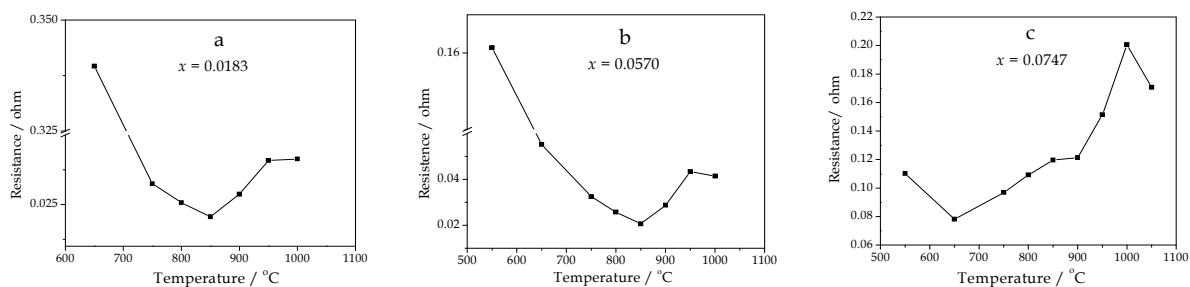


**Figure 14.** The variation of resistivity of nanocrystal with different content of Sb fired at different temperature.

Figure 14 shows the resistivity of Sb-doped  $\text{SnO}_2$  as a function of temperature. Fine powders with identical Sb content were fired at different temperatures; materials with different resistivities were obtained (Castro & Aldao, 2000; Morikawa & Fujita, 2000).

It is proposed that the variation in resistivity with temperature is associated with oxidation of Sb on the surface layer of the nanocrystal. The doping of Sb in a low-temperature regime yields only  $\text{Sb}^{+3}$ , leading to p-type doping. However, Sb on the surface layer in a high-temperature regime may yield  $\text{Sb}^{+5}$ , leading to n-type doping. Crystals grown at high temperatures are more perfect, so the resistivity of a crystal decreases. However, above  $850^\circ\text{C}$ , the number of  $\text{Sb}^{+5}$  ions on the surface layer increases, so the surface layer is transformed into an n-type. Semiconductors do not conduct electricity when they are connected in an n–p–n connection. So with the temperature increases, the n-type layer becomes thicker and the crystallites gradually transform into poorer conductors. Figure 14 also shows that more  $\text{Sb}^{+5}$  is formed at lower temperatures when the content of Sb is higher. Fig. 14 also indicates that the treatment at high temperature should be carefully adopted for the metal oxide with changeable valence.

#### 4.4. Solid superacid of Sb-SnO<sub>2</sub> nanocrystal

Hino & Kobayashi indicated at first in 1979 that the acid strength of the SO<sub>4</sub><sup>2-</sup>/ZrO<sub>2</sub> catalyst is estimated to be  $H_0$  (Hammett indicator)  $\geq -14.52$ , one of the strongest solid superacids. Sulfated zirconia (SO<sub>4</sub><sup>2-</sup>/ZrO<sub>2</sub>) is a typical solid superacid and exhibits a high catalytic activity for the skeletal isomerization of saturated hydrocarbons, and other reactions (Arata, 1990, 1996). Sulfated tin oxide (SO<sub>4</sub><sup>2-</sup>/SnO<sub>2</sub>) is one of the candidates with the strongest acidity on the surface. It has been reported that its acid strength is equal to that of SO<sub>4</sub><sup>2-</sup>/ZrO<sub>2</sub> at least (Matsushashi et al., 1989, 1990). Commonly, they have been prepared by the following procedures to generate superacidity (Matsushashi et al., 2001): (i) preparation of amorphous metal oxide gels as precursors; (ii) treatment of the gels with sulfate ion by exposure to a H<sub>2</sub>SO<sub>4</sub> solution or by impregnation with (NH<sub>4</sub>)<sub>2</sub>SO<sub>4</sub>; (iii) calcination of the sulfated materials at a high temperature in air.

The sulfated Sb-doped SnO<sub>2</sub> crystal is prepared in our study as follows. 2 g of Sb-doped SnO<sub>2</sub> powder obtained in Section 4.1 is placed in a 50 mL plastic centrifuge tube containing 45 mL of methanol. After the powder is dispersed on a shaker, 3.0 mL of saturated ammonium sulfate, equal to ~2 g of (NH<sub>4</sub>)<sub>2</sub>SO<sub>4</sub>, is added in methanol solution, and then the tube continues to be shaken on a shaker violently since once the saturated solution is dropped in methanol, very tiny (NH<sub>4</sub>)<sub>2</sub>SO<sub>4</sub> precipitate is separated in solution. After centrifugation, precipitate, a mixture of Sb-doped SnO<sub>2</sub> and (NH<sub>4</sub>)<sub>2</sub>SO<sub>4</sub>, is washed in anhydrous alcohol and centrifuged at 4000r/min. The final sediment is dried under an infrared ray lamp and a dispersed powder is obtained.

DTA-TG curves in Fig. 15 exhibits the thermo-gravimetric turn point of Sb-doped SnO<sub>2</sub> powder without mixing (NH<sub>4</sub>)<sub>2</sub>SO<sub>4</sub> is 376°C. Differential scanning calorimetry pattern shows the giving out heat peak is 341°C.

The relative acid strength of the powder was measured by the adsorption reaction of indicator. The powder (ca. 0.5 g) is calcined at 613 K in air for 3 h and then placed in a glass vacuum desiccator as the powder is hot. After the sample is pretreated in a vacuum for 2 h and cooled down to room temperature, some cyclohexane solution containing 5% of Hammett indicator is sucked in the vacuum desiccator. The desiccator is heated to 60 °C by placing it in a constant water bath, which results in the powder exposing to indicator vapor. The present powder sample is gradually colored by indicator and changes distinctly the colorless basic form of p-nitrotoluene ( $pK_a$  or  $H_0 = -11.4$ ), m-nitrotoluene (-12.0), m-nitrochlorobenzene (-13.2), and 2,4-dinitrotoluene (-13.8) to the yellow conjugate acid form and slightly yellow of 2,4-dinitrofluorobenzene (-14.5), that is to say, the acid strength of the solid acid is estimated at least to be  $H_0 \approx -14.5$ .

In the study, it is found that superficial hydroxyl on Sb-SnO<sub>2</sub> nanoparticles is very important for the sulfating roasting of Sb-SnO<sub>2</sub> nanocrystal. The fewer the number of superficial hydroxyl exist, the fewer the sulfated groups exist on the surface of Sb-SnO<sub>2</sub> nanocrystals. Compared with curves 1 (Sb-SnO<sub>2</sub>) and 8 (NH<sub>4</sub>)<sub>2</sub>SO<sub>4</sub>, curves 2 to 7 (Sb-SnO<sub>2</sub> + (NH<sub>4</sub>)<sub>2</sub>SO<sub>4</sub>) have an additional line segment from **a** to **b**. It is easy to understand that the line segment

implies the generation of superficially sulfated groups. Curves 2 to 7 are thermogravimetric curves of Sb-SnO<sub>2</sub> nanocrystals that are pretreated at different temperature for 3 h and then impregnated with a given amount of (NH<sub>4</sub>)<sub>2</sub>SO<sub>4</sub> before thermo-gravimetric analysis. It can be seen that the higher the preprocessing temperatures is, the shorter the line segments from **a** to **b** and the fewer the amount of sulfated group is. As the preprocessing temperature increases, especially at or over 341 °C, the weight losses of Sb-SnO<sub>2</sub> nanocrystals is heavier, which is contributed by the dehydration between hydroxyls, leading to dwindling in the number of superficial hydroxyls that are able to bond sulfate radicals and in the number of superficially sulfated groups and to decreasing acid strength or catalytic activities.

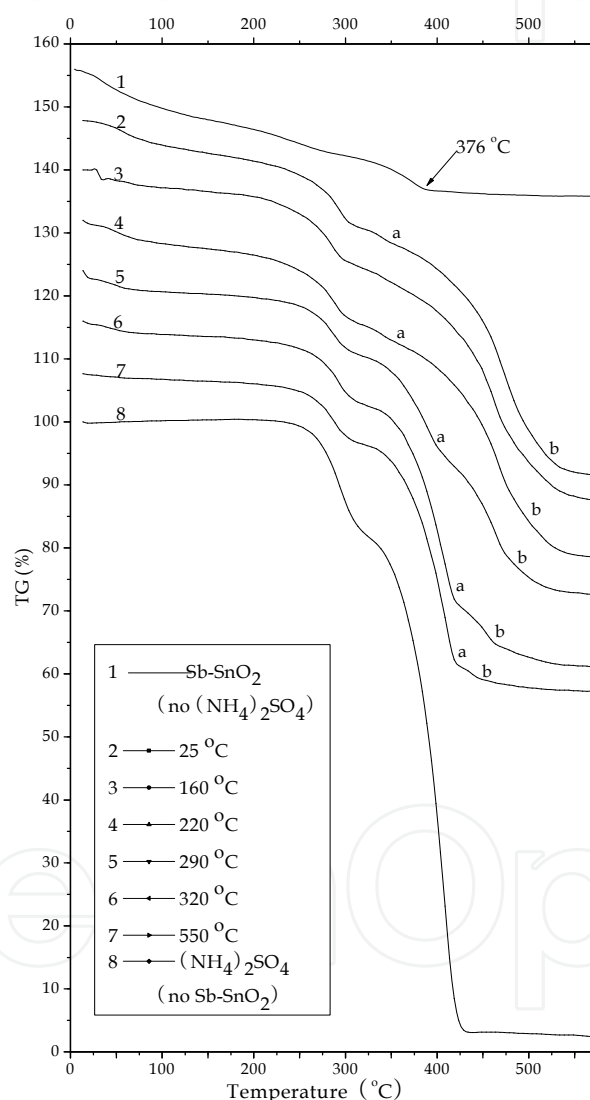


**Figure 15.** Thermogravimetric curves of Sb-SnO<sub>2</sub>, Sb-SnO<sub>2</sub> + (NH<sub>4</sub>)<sub>2</sub>SO<sub>4</sub>, and (NH<sub>4</sub>)<sub>2</sub>SO<sub>4</sub>.

Fig. 15 indicates that due to the generation of sulfated SnO<sub>2</sub>, the binding of SO<sub>4</sub><sup>2-</sup> on the SnO<sub>2</sub> endows the group with additional energy, so that to decompose or to volatilize the bonded SO<sub>4</sub><sup>2-</sup>, an excessive energy has to be provided in order to overcome the bonding force. Therefore line segments **a** to **b** appear in TG curves.



Fig. 15 substantiates the advantage that nanocrystal synthesized by the solution method has over the calcined nanocrystal in the surface modification of nanomaterials due to the existence of superficial hydroxyls.

## 5. Nanocrystal of zinc oxide and zinc oxide doped antimony or magnesium (Zhang et al., 2011, Liu et al., 2008)

Inorganic antimicrobial is a widely used as antibacterial material, which makes use of the blocking effect of metal ions and metal oxide to disinfect and decontaminate. Silver, as an inorganic antimicrobial, is widely known for its antibacterial properties against most of bacteria species. However, metal oxides, with higher stability in physics and chemistry and wide-spectrum and persistent antibacterial properties, show a high effective bactericidal potency at common circumstance. In particular, nano-sized inorganic antimicrobial expands the range of bactericidal application. Most inorganic antimicrobials are photocatalytic material, such as semiconductor:  $\text{TiO}_2$ ,  $\text{ZnO}$ ,  $\text{Fe}_2\text{O}_3$ ,  $\text{WO}_3$  and  $\text{CdS}$  etc. These materials can act with water under irradiation to produce non-selective and highly active hydroxyl radicals ( $\cdot\text{OH}$ ) that can kill or inhibit proliferation of microbe (Linsebiglar, et al., 1995, Stevenson, et al., 1997). Of them  $\text{ZnO}$  is an economic, resourceful, chemically stable and non-toxic photocatalytic antibacterial. Due to the low thermal expansion and cold contraction coefficients and highly chemical stability, zinc oxide is used in industrial and common living ceramics and also added to coating and paints.

### 5.1. Synthesis of nanocrystal of doped zinc oxide

In a flask containing 400 mL ethanol solution of a desired ratio of molar concentrations of  $\text{ZnCl}_2$  to  $\text{SbCl}_3$  or  $\text{MgCl}_2$  and 200 mL of anion exchange resin, 5 ~ 20 mL double-distilled water are added dropwise under stirring. The reaction is then conducted on a shaker and the solution containing suspended precipitate is separated with resin by a 120 mesh strainer. The filtrate containing precipitate reacts repeatedly five or six times with 50 mL fresh anion-exchange resin on a shaker until the upper solution does not become clear upon short standing (~ 2 h). The final chlorine-free solution is held idle on a bench for ca. 48 h. The upper lightly turbid solution is removed and kept aside. Iso-amyl acetate is added to the lower dense precipitate slurry. After mixed on a shaker for 120 min the mixture is dried in a glass distillation apparatus and a highly dispersive fine powder was obtained. All the reacted ion-exchange resins are combined and repeatedly washed with fresh solvent. The washed solvent is applied to a short column of ion exchange to remove any remaining chlorine, and is then combined with the upper lightly turbid solution. The dried powder from azeotropic distillation is dispersed in the combined solution on a shaker, and then distilled off the solvent and leave behind the fine powder with exactly dopant content.

### 5.2. The crystal structure of zinc oxide

The nanoparticle of  $\text{Sb-ZnO}$  and  $\text{Mg-ZnO}$  synthesized by the method of P-CNAIE associating with AD-IAA has a crystal structure even without calcining.

But it is discovered from Figure 16 that, when the doping level is higher than 1/10 (mole ratio), the crystal lattice of zinc oxide undergoes significant change. The XRD patterns of doping ratio at 1:5 for Mg-doped and Sb-doped ZnO crystals and 1:10 for Sb-doped ZnO indicate the formation of a new crystal phase. Moreover, Fig. 17, an enlarged figure, shows that the new crystal phase caused by Sb doping is different from that by Mg doping in crystal structure, which might be one of major causes that lead to a difference in bacteriostatic potency between Mg-doped and Sb-doped ZnO nanocrystals. The Mg doping contributed to 5 new XRD peaks appear at  $17.0^\circ$ ,  $22.4^\circ$ ,  $25.5^\circ$ ,  $28.6^\circ$  and  $38.3^\circ$  ( $2\theta$ ), while the Sb doping brought on 3 new peaks at  $17.0^\circ$ ,  $24.6^\circ$  and  $38.3^\circ$  ( $2\theta$ ). (See Fig. 17).

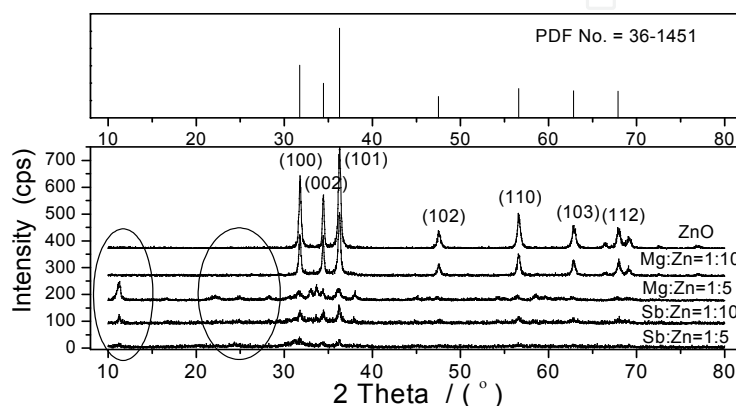


**Figure 16.** XRD patterns of ZnO nanoparticle doped with  $\text{Sb}^{3+}$  or  $\text{Mg}^{2+}$ . The up patterns is the X-ray powder diffraction standards, PDF No. 36-1451, of ZnO from Jade 5.0.

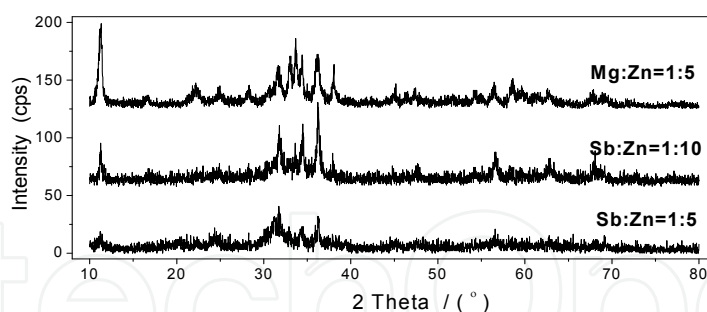


**Figure 17.** XRD patterns of ZnO nano-particle doped with  $\text{Sb}^{3+}$  or  $\text{Mg}^{2+}$  at heavy doping.

Variation of the structure of doped ZnO can be seen under an electron microscope. TMS images indicate such variation induced by doping Mg and Sb. Fig. 18A and E show non-doped ZnO with a structure of typical columnar crystal and bigger size. In the case of doping, the size of Sb-doped ZnO crystal evidently decreased with Sb content increasing, as Fig. 18B, C and D show. It can be seen from Fig. 18C and D that besides many short columnar crystal a great deal is grained crystal. However, as Mg is doped into ZnO, the crystal size does not change a lot, but the crystalline form varies from six-rowed columnar to six-rowed lamellar. The lamellar crystal appears in very small amount as doping level is low (see Fig. 18E, indicated by arrow), and in a great amount as doping ratio reached to 1 : 5 (see Fig. 18F).

The outer-shell valence electrons of zinc atoms are four (2s and 2d) and its ionic radius 0.60 Å, the valence electrons of magnesium are two (2s) and ionic radius only 0.57 Å, while that of antimony are five (2s and 3p) and the ionic radius up to 0.74 Å. Therefore, when the doping is heavy, the effects of differences in the number of outer-shell electrons and in the ionic radius on the variation in crystal form are more distinct, contributing to the transformation of original six-rowed columnar crystals into new crystal form.

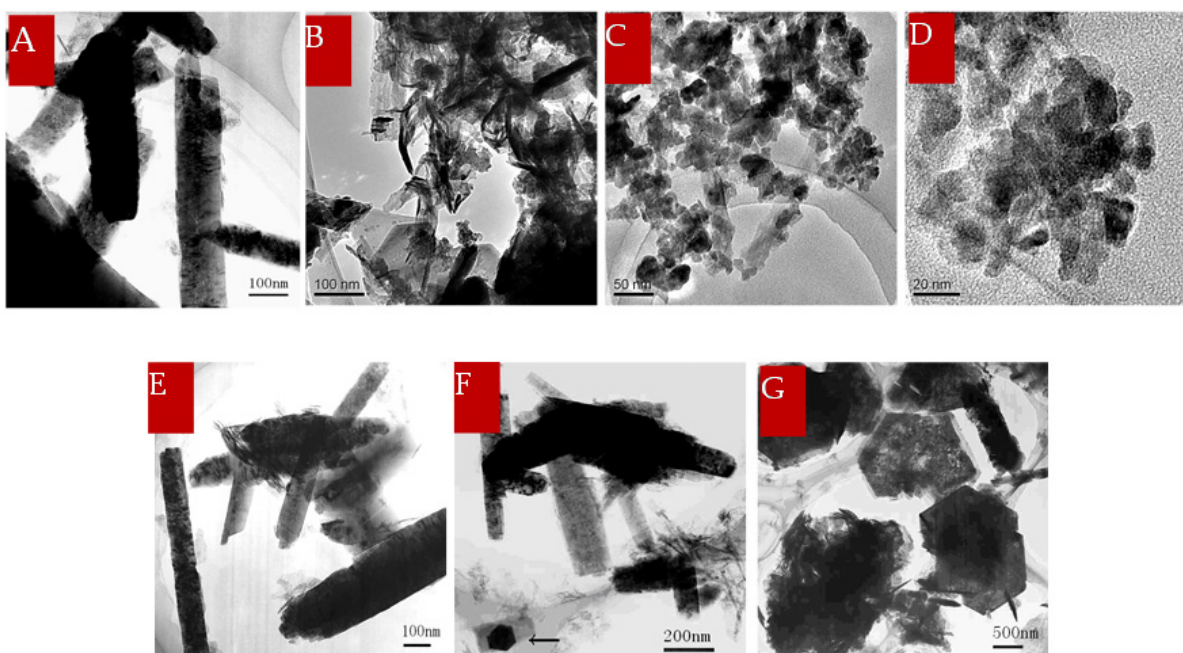


**Figure 18.** TEM (JEM-2010 (HT), JEOL, Japan) images of doped and non-doped zinc oxides. A is a pure ZnO, B: Zn : Sb = 1:15, C: Zn : Sb = 1:10 and D: Zn : Sb = 1:5. The low group, E is a pure ZnO, F: Mg : Zn = 1:10 and G: Mg : Zn = 1:5.

When element Mg(II) is doped into matrix element Zn(II), both of them have the same valence and the same ratios of metal atom to oxygen atom, which will not cause any hanging bonds within crystal, but the distortion of lattice resulted from the difference in ionic radius between matrix and doping elements at heavy doping lead to the formation of hanging bond and hence an enhancement of photo-catalysis of the doped crystal. Whereas in the case of Sb doping, Sb(III) has one more oxygen atom around it than Zn(II), which causes a hanging bond on Sb atom, or a unbonding valence electron. This unbonding electron becomes a free electron within crystal lattice, resulting in the number of free electron more than the number of positive hole and becoming a n-type semiconductor. As is well known, ZnO crystal is a n-type semiconductor. Consequently, Sb-doping promotes the semiconductor characteristic of ZnO, endowing it a more effective photo-catalysis. In addition, the difference in ionic radius also assisted the distortion of crystal lattice, so the variation of ZnO crystal as antimony dopes is more obvious than as magnesium dopes.

A relevant doping, as at 1/10, is important for to maintain ZnO's semiconductive nature as well as its basic columnar structure. The main change is the particle size (Fig. 18C and the

arrow pointed in F). Such doping provides the nanomaterial an enhanced semiconductive characteristic and effective photo-catalysis. The formation of new crystal, as XRD peak at  $17.0^\circ$  shows, does not much help to increase the photo catalysis, or bactericidal potency because, we supposed, the bactericidal potencies at doping ratio of over 1/5 are much lower than these at doping ratio of 1/10. Maybe the new crystal is not a semiconductor and hence can not produce hydroxyl free radical when it acts with water at irradiating.

### 5.3. The bactericidal properties

The bacteriostatic rate of Sb-doped ZnO nano powder is only 12% as the plats are incubated in darkness. While check experiments of Sb-doped ZnO powder are carried out under lighting, which leads to a bactericidal rate up to 93.4%, increasing by over 80%. The Mg-doped ZnO powder improves its bacteriostatic rate from 9.8% without irradiating to 83.5%. Fig. 19 shows that the doped materials have a much high antibacterial performance than non-doped materials at both irradiating and darkness conditions. Among tested nanomaterials, Sb-doped crystal presents the highest bactericidal potency, while the potency from non-doped material is the lowest. Meanwhile, the irradiation enhances antibacterial rate of all tested nano crystals. The light does play a vital role on the antibacterial behaviors of tested nanomaterials, because of the limited antimicrobial properties in darkness. We supposed that such antibacterial behaviors are due to the reactions between nanocrystal and water molecule under visible-light irradiation to produce free radical. The antibacterial behavior caused by irradiating disappears once the irradiation is removed. The limited bactericidal potency under darkness might be caused by the limited amount of free radical that is produced by powder absorbing environmental energy to act with water molecule.

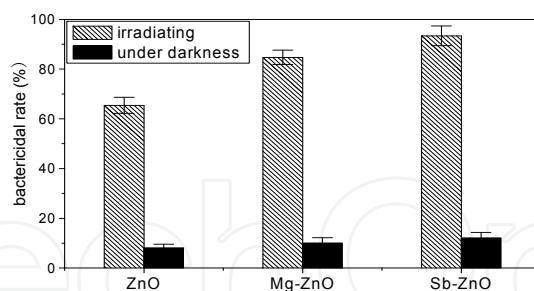
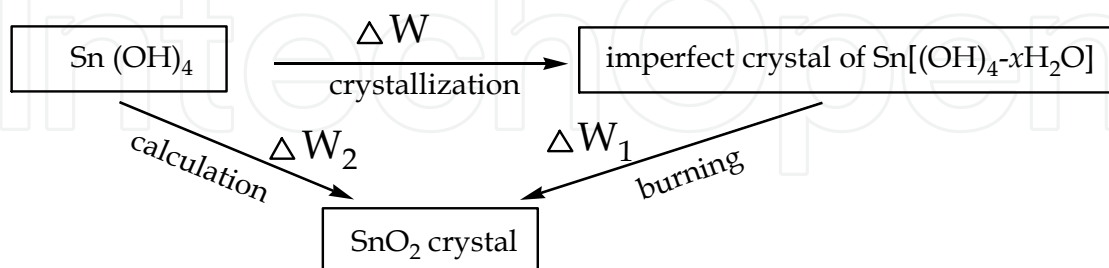


**Figure 19.** The lighting culture test of different nano ZnO powders on *E. coli*. Dark bars show the incubation under non-irradiate and bias bars under irradiate. The doping ratio of Mg-doped ZnO and Sb-doped ZnO are 1/10.

## 6. Calculation of crystallinity, $\bar{X}_n$ , of Nanocrystal synthesized by solution method (Zhang et al., 2005, 2006, 2009)

Metal hydroxide can be burned at high temperature, and water loss has it transformed into an oxidate. So the remained metal hydroxide that dose not condensate to form oxidate crystal can be calculated by weighing water loss as the superficial metal hydroxide is

burned. A simple and reliable method to determine the number of water molecules, a by-product in the polycondensation of metal hydroxide into metal oxide crystal, is proposed in order to calculate the average crystallinity of nanocrystal synthesized by solution method. The number of water molecules can be determined by weighing the difference between synthesized nanocrystals before and after burning. There is a close circle relationship (tin in this calculation example), by which the average crystallinity can be calculated.



**Scheme 3.** The conversion relationship of monomer, polycondensate and crystal, and the cyclic relationship of calculation of water molecule numbers.

$$\text{No. of water molecules} = \frac{\Delta W}{M_{\text{H}_2\text{O}}} = \frac{\Delta W_2 - \Delta W_1}{M_{\text{H}_2\text{O}}}$$

Here,  $\text{Sn}(\text{OH})_4$  and  $\text{SnO}_2$  have definite molecular weights and can be calculated or experimentally determined. So the number of water molecules produced as condensation, or crystallization, is given. Being divided by a parameter  $n_0$ , which is the number of tin atom or monomer  $\text{Sn}(\text{OH})_4$ , the equation changes as follow and the  $n_0$  can be described as Eq. (10),

$$\frac{(\text{No. of water molecules}) \times M_{\text{H}_2\text{O}}}{n_0} = \frac{W_{\text{Sn}(\text{OH})_4}}{n_0} - \frac{W_{\text{polycondensate}}}{n_0}$$

$$n_0 = \frac{(\text{No. of water molecules}) \times M_{\text{H}_2\text{O}}}{M_{\text{Sn}(\text{OH})_4} - M_{\text{polycondensate}}} \quad (10)$$

Here  $W_{\text{polycondensate}}$  stands for  $W_{\text{imperfect crystal of Sn}[(\text{OH})_4-x\text{H}_2\text{O}]}$  or  $W_{\text{Sn}[(\text{OH})_4-x\text{H}_2\text{O}]}$ . And the number of end groups of the polycondensate molecules is given by

$$\text{No. of end hydroxyl groups of imperfect crystal} = 2 \times \frac{\Delta W_1}{M_{\text{H}_2\text{O}}}$$

The extent of conversion,  $r'$ , that is, polycondensate, or imperfect crystal converts into perfect crystal of  $\text{SnO}_2$ :

$$r' = W_{\text{SnO}_2}^* / W_{\text{polycondensate}}^* = n_0 \times M_{\text{SnO}_2} / n_0 \times M_{\text{Sn}[(\text{OH})_4-x\text{H}_2\text{O}]}$$

And so



$$M_{\text{Sn}[(\text{OH})_4-x\text{H}_2\text{O}]} = M_{\text{SnO}_2} / r' \quad (11)$$

where  $W^*_{\text{polycondensate}}$  and  $W^*_{\text{SnO}_2}$  are the masses of the imperfect crystal to be fired and of the oxide formed after firing, respectively. The extent of theoretical conversion is:

$$W_{\text{SnO}_2} / W_{\text{Sn}(\text{OH})_4} = M_{\text{SnO}_2} / M_{\text{Sn}(\text{OH})_4} = R < r'$$

because the condensation results from intermolecular elimination of water and hence  $M_{\text{Sn}(\text{OH})_4} > M_{\text{Sn}[(\text{OH})_4-x\text{H}_2\text{O}]}$ . Substituting Eq. (11) for  $M_{\text{Sn}[(\text{OH})_4-x\text{H}_2\text{O}]}$  in the expression Eq.(10), a general expression is given as Eq. (12)

$$n_0 = \frac{(\text{No. of water molecules}) \times M_{\text{H}_2\text{O}}}{M_{\text{Sn}(\text{OH})_4} - \frac{M_{\text{SnO}_2}}{r'}} \quad (12)$$

Once the number of water, or the number of condensation reactions, is given, the  $n_0$  can be calculated using  $r'$ . The  $n_0$  will only be the function of  $r'$ . With  $r'$  increases, the number of initially presented monomer,  $n_0$ , should be less, meaning the degree of condensation increase. For convenience's sake, the number of condensation reactions, or No. of water molecules, can be factitiously set on requirement of calculation accuracy, say 100, 1,000, 10,000 and so on. Its significance is that in each  $n_0$  of monomers, intermolecular condensations occur by the elimination of a certain water molecules between monomers. The definition of the  $n_0$  is the number of initially presented monomer or the total molar number of metal elements.

**For example:** In the preparation of Sb-doped  $\text{SnO}_2$ ,  $W^*_{\text{Sn}(\text{OH})_4} = 0.9573$  g,  $W^*_{\text{SnO}_2} = 0.8836$  g and so  $r'$  is 0.9320. In addition,  $M_{\text{Sn}(\text{OH})_4} = 186.71$ ,  $M_{\text{SnO}_2} = 150.71$ ,  $M_{\text{H}_2\text{O}} = 18.002$ . So the Eq. (12) is written as follows when the No. of water molecules is set as 1,000.

$$n_0 = \frac{18.002 \times 1000}{186.71 - \frac{150.71}{0.9230}} = 768$$

It indicates that 768 of hydroxides take place 1,000 condensation reactions by losing 1,000 water molecules. According to the definitions of the average degree of polymerization,  $\bar{X}_n$ , which here should be called as the average crystallinity, the expression is

$$\bar{X}_n = \frac{\text{No. of units}}{\text{No. of polymers}} = \frac{N_0}{N}$$

For linear condensation, including side-chain condensation, the average effective functionality (i.e. the number of condensable functional groups) of every monomer is supposed to be two, i.e.  $\bar{f} = 2$ , and the equation of Carothers can be directly used to calculate the average degree of polymerization,  $\bar{X}_n$ .



$$p = (N_0 - N) / N_0 = 1,000 / n_0$$

$$\bar{X}_n = 1 / (1 - p) = n_0 / (n_0 - 1,000) \quad (13)$$

where  $p$  is the extent of reaction, and  $N_0$  and  $N$  are respectively the total numbers of molecules initially and finally present, respectively.  $(N_0 - N) = 1,000$  (water molecules) and  $N_0 = n_0$ . For  $n_0 = 2000$ ,  $\bar{X}_n = 2$ ;  $n_0 = 1125$ ,  $\bar{X}_n = 9$  and  $n_0 = 1000$ ,  $\bar{X}_n = \infty$ . See the  $\bar{X}_n$  in Table 3. For nonlinear condensation, products have a network structure, which, conceivably, might be a planar network analogous to that of graphite, or a space network analogous to that of diamond. Compared and analyzed a great number of typical structural units, values of  $\bar{X}_n$  in this case can be obtained using expressions,

$$N = 2 \times 1000 / (\bar{X}_n \bar{f} - \sqrt{\bar{X}_n} \bar{f})$$

$$\bar{X}_n = N_0 / N = \left[ N_0 \bar{f} / (N_0 \bar{f} - 2 \times 1000) \right]^2 = \left[ n_0 \bar{f} / (n_0 \bar{f} - 2 \times 1000) \right]^2 \quad (14)$$

where  $\bar{X}_n \bar{f}$  refers to the total number of functional groups before condensation,  $\sqrt{\bar{X}_n} \bar{f}$  is the number of unreacted groups remaining within the structure units after condensation, and  $2 \times 1000$  is the number of reacted groups. As  $n_0 = 1000$ ,  $\bar{X}_n = 4$ ;  $n_0 = 750$ ,  $\bar{X}_n = 9$ ;  $n_0 = 667$ ,  $\bar{X}_n = 16$ ; and  $n_0 = 500$ ,  $\bar{X}_n = \infty$ .

$r'$ (%)	$n_0 \times 1000$	$\bar{X}_{n(\text{linear})} \dagger$	$\bar{X}_{n(\text{net-linear})} \dagger$	$\bar{X}_{n(\text{space-net})} \dagger$
80.72	$\infty$	Single	Single	Single
80.75	225025			
80.8	94747			
81	27695			
82	6165			
84	2651			
84.80	2000	2		
87.46	1250	5		
88.28	1125	9		
88.77	1063	17		
89.14	1020	50		
89.33	1000	$\infty$	2	4
92.63	750		3	9
94.36	667		4	16
97.43	562		9	81
98.54	533		16	256
99.54	509		49	2401
100	500		$\infty$	$\infty$

†: Assuming only one kind of structural unit is yielded in the condensation.

**Table 3.** The  $\bar{X}_n$ , crystallinity, corresponding with  $r'$  and  $n_0$ .

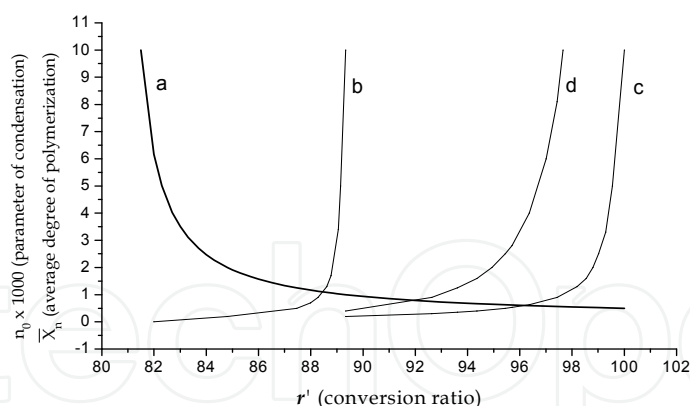


**Figure 20.** In a given condensation reaction, the relation, denoted as a, between  $n_0$  and  $r'$  according to Eq. (12), and the relations, denoted as b, c and d, between  $\bar{X}_n$  and  $r'$  according to Eqs. (13) and (14), respectively.

## Author details

Xuejun Zhang

*School of Chemistry and Chemical Engineering, Guizhou University, Guiyang, Guizhou, China*

Fuxing Gan

*School of Resource and Environmental Science, Wuhan University, Wuhan, Hubei, China*

## Acknowledgement

The authors thank Dr. Fen Yang, Dr. Hua Zhu, Dr. Xuhui Ma, Peng Liu, Liye Fu, Rong Zhou, Hanmei Ouyang and Hui Zhong for participating in parts of experimental work, and give many thanks to Prof. Chris Abell of the Chemistry Department, University of Cambridge, for the correction on part of manuscript. We are extremely thankful to the “Chun Hui” Project of the Ministry of Education of China for funding this research.

## 7. References

- Arata, K. (1990). Solid Superacides. *Adv. Catal.* Vol.37, pp. 165-211. ISSN: 0360-0564
- Arata, K. (1996). Preparation of superacids by metal oxides for reactions of butanes and pentanes. *Appl. Catal, A: General*, No.146, pp. 3-32.
- Brinker, C. J. & Scherer, G. W. (1990). *Sol–Gel Science: The Physics and Chemistry of Sol–Gel Processing*, pp. 89–103. Academic Press, Boston, and references therein.
- Boujday, S. Wünc, F. Portes, P. Bocquet, J-F. and Christophe, C-J. (2004). Photocatalytic and Electronic Properties of TiO<sub>2</sub> Powder Elaborated by Sol–Gel Route and Supercritical Drying. *Sol. Energy Mater. Sol. Cells*, Vol.83, No.4, pp. 421–33.
- Cao, X. Cao, L. Yao, W. & Ye, X. (1998). Influence of Dopant on the Electronic Structure of SnO<sub>2</sub> Thin Films. *Thin Solid Films*, Vol.317, No.2, pp. 443–5.

- Castro, M. S. & Aldao, C. M. (2000). Effects of Thermal Treatments on the Conductance of Stannic Oxide. *J. Eur. Ceram. Soc.*, Vol.20, No.3, pp. 303–7.
- Diao, Y. Walawender, W. P. M. Sorensen, C. Klabunde, K. J. & Ricker, T. (2002). Hydrolysis of Magnesium Methoxide. Effects of Toluene on Gel Structure and Gel Chemistry. *Chem. Mater.*, Vol.14, No.1, pp. 362–8.
- D'Souza, L. Suchopar, A. & Richards, R. M. (2004). In Situ Approaches to Establish Colloidal Growth Kinetics. *J. Colloid Interf. Sci.*, No.279, pp.458–63.
- Frazee, J. & Harris, T. (2001). Processing of Alumina Low-Density Xerogels by Ambient Pressure Drying. *J. Non-Cry. Sol.*, Vol.285, No.1–3, pp. 84–9.
- Gržeta B. Tkalc̃ec E. Goebbert C. Takeda M. Takahasgi M. Nomura K. & Jaksic M. (2002). Structural Studies of Nanocrystalline SnO<sub>2</sub> Doped with Antimony: XRD and Mössbauer Spectroscopy. *J. Phys. Chem. Solids*, Vol.63, No.2, pp. 765–72
- Hino, M. Kobayashi, S. & Arata, K. (1979). Reactions of Butane and Isobutane Catalyzed by Zirconium Oxide Treated with Sulfate Ion. Solid Superacid Catalyst, *J. Am. Chem. Soc.* No.101, pp. 6439–6441
- Hu, Z. Dong, J. & Chen, G. (1998). Replacing Solvent Drying Technique for Nanometer Particle Preparation. *J. Colloid Interface Sci.*, Vol.208, No.2, pp. 367–72.
- Hwang, K.-T. Auh, K.-H. Kim, C.-S. Cheong, D.-S. & Niihara, K. (1997). Influence of SiC Particle Size and Drying Method on Mechanical Properties and Microstructure of Si<sub>3</sub>N<sub>4</sub>/SiC Nanocomposite. *Mater. Lett.*, Vol.32, No.4, pp. 251–7.
- Irvin, J. C. (1962). Resistivity of Bulk Silicon and of Diffused Layers in Silicon. *Bell Systems Tech. J.*, No.41, pp. 387–91.
- Linsebigler, A. Lu, G. & Yates, J. Jr. (1995), Photocatalysis on TiO<sub>2</sub> surfaces-principle, mechanisms, and selected results, *Chem Rev*, Vol95, No.3, pp. 735–758.
- Liu, P. Guo, Z. Zhang, X. & Xiao, T. (2008). Novel Anion Exchange Method for Synthesis of Zinc Oxide Nanocrystal Powder and Photocatalytic Activity of the Powder, *Nanoscience & Nanotechnology (China)*, Vol.5, No.1, pp. 64–69.
- Luliang, Q. Yongcun, L. & Yang, X. (2000). *Handbook of Chemicals and Materials for Treatment of Water*. p. 217. China Petrol and Chemistry Publishing House, Beijing.
- Luan, W.-L. Gao, L. & Guo, J.-K. (1998). Study on Drying Stage of Nanoscale Powder Preparation. *Nanostructured Mater.*, Vol.10, No.7, pp. 1119–25.
- Matsushashi, H. Hino, M. & Arata, K. (1989). In Acid-Base Catalysis; Tanabe, K., Hattori, H., Yamaguchi, T., Tanaka, T., Ed. p 357. Kodansha: Tokyo.
- Matsushashi, H. Hino, M. Arata, K. (1990). Solid catalyst treated with anion: XIX. Synthesis of the solid superacid catalyst of tin oxide treated with sulfate ion. *Appl. Catal.* Vol.59, No.1, pp. 205–212.
- Matsushashi, H. Miyazaki, H. Kawamura, Y. Nakamura, H. and Arata, K. (2001). Preparation of a Solid Superacid of Sulfated Tin Oxide with Acidity Higher Than That of Sulfated Zirconia and Its Applications to Aldol Condensation and Benzoylation<sup>1</sup>, *Chem. Mater.* No.13, pp. 3038–3042

- Morikawa, H. & Fujita, M. (2000). Crystallization and Electrical Property Change on the Annealing of Amorphous Indium-Oxide and Indium-Tin-Oxide Thin Films. *Thin Solid Films*, Vol.359, No.1, pp. 61–7.
- Park, C. Bell, A. T. & Tilley, T.T.D. (2002). Oxidative Dehydrogenation of Propane Over Vanadia–Magnesia Catalysts Prepared by Thermolysis of  $\text{OV}(\text{OtBu})_3$  in the Presence of Nanocrystalline  $\text{MgO}$ . *J. Catal.*, Vol.206, No.1, pp. 49–59.
- Richards, R. & Khaleel, A. (2001). Ceramics, in: *Nanoscale Materials in Chemistry*, K. J. Klabunde, (Ed), pp. 95–9, Wiley VCH, New York.
- Richards, R. Mulukutla, R. Volodin, A. Zaikovski, V. Sun, N. & Klabunde, K. (2001) Nanocrystalline Ultra High Surface Area Magnesium Oxide as a Selective Base Catalyst. *Scripta Materialia*, Vol.44, No.8–9, pp. 1663–6.
- Shlyakhtin, O. Oh, Y-J. & Tretyakov, Y. (2000). Preparation of Dense  $\text{La}_{0.7}\text{Ca}_{0.3}\text{MnO}_3$  Ceramics from Freeze-Dried Precursors. *J. Eur. Ceram. Soc.*, Vol.20, No.12, pp.2047–54.
- Stevenson, M. Bullock, K. & Lin, W. (1997). Sonolytic enhancement of the bactericidal activity of irradiated titanium dioxide suspensions in water. *Res Chem Intermed*, Vol.23, No.4, pp. 311–323.
- Sun, C. and Berg, J. C. (2002). Effect of Moisture on the Surface Free Energy and Acid–Base Properties of Mineral Oxides. *J. Chromatogr. A*, Vol.969, No.1–2, pp. 59–72.
- Wuhan University (Yang, D. Meng F. Pan Z. Ni Q. & Li G. Ed). (2000). *Analytical Chemistry*, 4th edition, p. 339 and pp. 184–5, Higher Education Press, Beijing, (Chinese).
- Vidal, K. Lezama, L. Arriortua, M. Rojo, T. Gutie'rrez, J. & Barandiarán, J. (2005). Magnetic Characterization of  $\text{Nd}_{0.8}\text{Sr}_{0.2}(\text{Mn}_{1-x}\text{Co}_x)\text{O}_3$  Perovskites," *J. Magn. Magn. Mater.*, Vol.290–291, No.4, pp. 914–6.
- Yang, F. Zhang, X. Mao, X & Gan, F. (2007). Synthesis and Characterization of Highly Dispersed Antimony-Doped Stannic Hydroxide Nanoparticles: Effects of the Azeotropic Solvents to Remove Water on the Properties and Microstructures of the Nanoparticles, *J. Am. Ceram. Soc.*, Vol.90, No.4, pp. 1019–1028.
- Yoffe, D. (1993). Low-Dimensional Systems: Quantum Size Effects and Electronic Properties of Semiconductor Microcrystallites (Zero-Dimensional Systems) and Some Quasi-Two-Dimensional Systems. *Adv. Phys.*, Vol.42, No.2, pp. 173–266.
- Zhang, X. (2005). The Preparation and Electrochemical Properties of Sb-Doped Stannic Oxide Nanocrystal. Doctoral Dissertation, Wuhan University, Wuhan, Hubei, China..
- Zhang, X. Fu, L. Zhang, M. & Guo, Z. (2008). Solution Method for Synthesizing Nanocrystal of Metal Oxide, *J. Material & Engineering* (China), No.10, pp. 157–163.
- Zhang, X. Liang, H & Gan, F. (2006). Novel Anion Exchange Method for Exact Antimony Doping Control of Stannic Oxide Nanocrystal Powder. *J. Am. Ceram. Soc.*, Vol.89, No.3. pp. 792–798
- Zhang, X. Guo, Z. Zhang, M. & Fu, L. (2009). Parameters of Condensation of Sb-Doped Stannic Hydroxide and Their Correlation with Nano-Crystalline Sb-Doped Stannic Oxide *J. Sci. Conf. Proc.* Vol.1, pp. 258–267

Zhang, X. Zhou, R. Liu, P. Fu, L. Lan, X. & Gong, G. (2011). Improvement of the Antibacterial Activity of Nanocrystalline Zinc Oxide by Doping Mg (II) or Sb (III) *Int. J. Appl. Ceram. Technol.*, Vol.8, No.5, pp. 1087–1098

IntechOpen

IntechOpen